Elsevier Editorial System(tm) for Advances in Space Research

Manuscript Draft

Manuscript Number: JASR-D-04-00608R1

Title: Title of Manuscript:-
Optimising Estimates of Mesospheric Neutral Wind Using the TIGER SuperDARN Radar

COSPAR Paper Number from Final Programme:- CO.2-0020-04
(COSPAR04-A-01665)

Article Type: Contributed Paper

Section/Category: C0.2 Advances in Remote Sensing of the Middle and Upper Atmosphere and Ionosphere

Keywords: Neutral Winds; Meteors; TIGER

Corresponding Author: Miss Deanna Matthews, BSci(Hons)

Corresponding Author's Institution: LaTrobe University

First Author: Deanna Matthews, BSci(Hons)

Order of Authors: Deanna Matthews, BSci(Hons); Murray L Parkinson, PhD; Peter L Dyson, PhD

Manuscript Region of Origin:

Abstract:
Optimising Estimates of Mesospheric Neutral Wind Using the TIGER SuperDARN Radar

D. M. Matthewsa, M. L. Parkinsona, P. L. Dysona, and J. C. Devlinb

aDepartment of Physics, La Trobe University, Melbourne, Victoria 3086, Australia

bDepartment of Electronic Engineering, La Trobe University, Victoria 3086, Australia

Abstract

Super Dual Auroral Radar Network (SuperDARN) HF backscatter radars scan 16 beam directions over a field of view of ~52°. In the common mode of operation, data is collected using 45-km range gates and 7-s integrations on each beam. Application of a beam-swinging algorithm permits mesospheric neutral winds to be estimated from the line-of-sight (LOS) Doppler velocity of meteor echoes detected at near ranges (<600 km). Larger meteor echo detection rates better constrain the solutions and thereby increase the accuracy of wind estimates. Greater rates also lead to wind estimates with better time and height resolution. In this study, meteor echo detection rates were increased by running dedicated radar control programs on the Tasman Geospace Environment Radar (TIGER) Tasmania radar (147.2°E, 43.4°S). This involved the use of shorter 15-km range gates and 2-s integration times. The Doppler characteristics of different echo types at meteor echo ranges were identified. The echoes were then filtered according to these characteristics, and their suitability for estimating neutral winds investigated. One echo type was clearly of ionospheric origin, forming thin, continuous traces decreasing in group range from ~1200 km to ~300 km before midnight. These "descending plasma streams" (DPS) merged into and contaminated the meteor scatter observed by TIGER. However, they will be less of a problem for the planned network of "storm time" SuperDARN radars to be deployed at mid-latitudes for the study of major substorms and storms which occur less frequently.

Optimising Estimates of Mesospheric Neutral Wind Using the TIGER SuperDARN Radar

D. M. Matthews[a], M. L. Parkinson[a], P. L. Dyson[a], and J. C. Devlin[b]

[a]*Department of Physics, La Trobe University, Melbourne, Victoria 3086, Australia*
[b]*Department of Electronic Engineering, La Trobe University, Victoria 3086, Australia*

Abstract

Super Dual Auroral Radar Network (SuperDARN) HF backscatter radars scan 16 beam directions over a field of view of ~52°. In the common mode of operation, data is collected using 45-km range gates and 7-s integrations on each beam. Application of a beam-swinging algorithm permits mesospheric neutral winds to be estimated from the line-of-sight (LOS) Doppler velocity of meteor echoes detected at near ranges (<600 km). Larger meteor echo detection rates better constrain the solutions and thereby increase the accuracy of wind estimates. Greater rates also lead to wind estimates with better time and height resolution. In this study, meteor echo detection rates were increased by running dedicated radar control programs on the Tasman Geospace Environment Radar (TIGER) Tasmania radar (147.2°E, 43.4°S). This involved the use of shorter 15-km range gates and 2-s integration times. The Doppler characteristics of different echo types at meteor echo ranges were identified. The echoes were then filtered according to these characteristics, and their suitability for estimating neutral winds investigated. One echo type was clearly of ionospheric origin, forming thin, continuous traces decreasing in group range from ~1200 km to ~300 km before midnight. These "descending plasma streams" (DPS) merged into and contaminated the meteor scatter observed by TIGER. However, they will be less of a problem for the planned network of "storm time" SuperDARN radars to be deployed at mid-latitudes for the study of major substorms and storms which occur less frequently.

1. Introduction

The mesosphere-lower thermosphere (MLT) is a relatively inaccessible atmospheric region because it is too high to be probed using *in situ* radiosondes, yet too low to be probed using *in situ* satellites. However, understanding the dynamics of gravity waves, tides, and planetary waves within the MLT region has important implications for the chemistry and dynamics of the stratosphere (Viereck, 1991). Although dedicated VHF meteor radars provide measurements of winds within the MLT, opportunities exist to extend the spatial coverage around Earth using other radar systems, such as ionosondes (MacDougall et al., 2001), and via the use of remote sensing satellites such as the Thermosphere, Ionosphere, Mesosphere, Energetics and Dynamics (TIMED) mission.

The Tasman International Geospace Environment Radar (TIGER) (Dyson and Devlin, 2000) is a pair of SuperDARN radars located in Tasmania and New Zealand. This study uses data obtained by TIGER Tasmania (147.2°E, 43.4°S) prior to the deployment of the New Zealand radar. SuperDARN radars were designed to detect ionospheric backscatter and were deployed to study the dynamics of the high-latitude ionosphere (Greenwald et al., 1995). However, SuperDARN radars also detect echoes from other sources such as the ground and the sea, and from meteors. The radars are being upgraded with hardware and software to facilitate simultaneous data acquisition for the study of these various phenomena.

Hall et al. (1997) identified Grainy Near Range Echoes (GRNEs) in SuperDARN data. GRNEs occur at ranges less than ~500 km and are present regardless of magnetic activity. GNRE detection rates peak near local dawn and reach a minimum near local dusk, paralleling the diurnal variation of meteors observed optically and with VHF meteor radars. Hall et al. (op cit) concluded GRNEs were due to backscattering from meteor trails. The characteristics of SuperDARN meteor echoes have been further investigated by various authors (e.g. Jenkins and Jarvis, 1999; Hussey et al., 2000; Arnold et al., 2001; Arnold et al., 2003).

Classical VHF meteor radars rely on the observation of underdense meteors, identified by their rapid rise time and subsequent exponential decay. Such meteor trails have a well known diffusion relationship (Arnold et al., 2001) and travel with the background wind. Overdense meteors, on the other hand, do not necessarily diffuse and merge into the atmosphere, drifting with the neutral wind. Depending on the size, density and composition of the meteorite, its ablation can modify the chemistry and dynamics of the atmosphere. In the worse case, the radar echoes can consist of multiple, interfering total reflections exhibiting Doppler shifts unrelated to the background wind. Overdense meteor echoes were not rejected in the present study, but our results suggest the echoes were predominately from structures drifting at the background wind speed.

The identification of meteor echoes in SuperDARN data is important because the Doppler shift of these echoes can be used to determine the neutral wind in the MLT region, and the number and locations of SuperDARN radars can provide a significant extension of the available observations. As Table 1 shows, meteor echoes are basically identified as echoes at short range, from D- and E-region heights, and with low line-of-sight (LOS) Doppler velocity and spectral width. However the population of echoes with these characteristics may include some ionospheric echoes as well. Furthermore, the likelihood of detecting meteor echoes will depend on the choice of radar operating parameters. These are usually chosen to detect F-region ionospheric echoes, not meteor echoes.

The TIGER Tasmania radar was used to examine the extent to which meteor echo detection rates depend on radar operating parameters including the frequency and integration time. The characteristics of the near range echoes were studied to aid separation of meteor echoes from the broader population of radar echoes. The echo detection rates were greatly improved, thereby permitting the calculation of neutral winds with better accuracy and time resolution than obtained using the standard radar operating mode and analysis.

2. Observations and Analysis

In normal operations, SuperDARN radars scan 52° of azimuth by electronically stepping the radar beam through 16 steps or beam directions separated by 3.24°. The transmitter pulse width usually corresponds to 45 km of range, and the first range gate is 180 km, with 70 more ranges separated by 45 km. The transmitter frequency is often ~12 MHz or less, and the integration time is typically 7 s. The backscatter power (dB), LOS velocity (m s^{-1}), and spectral width (m s^{-1}) of echoes are estimated in real time using a standard pulse set scheme and analysis algorithm. The spectral widths are a measure of the spread of LOS Doppler velocity in the sampling volume which is determined by the beam width and pulse width. The standard method of running the radars is appropriate for the measurement of ionospheric scatter out to great ranges.

Several special campaigns were run using the TIGER radar to specifically investigate meteor echoes. Beam 7 points near to geographic south and Figure 1 shows results obtained along this beam for a 56-hour campaign lasting from 00 hours LT, 24 May to 08 LT, 26 May 2003 (LT=UT+10 hours). During an integration period, the radar takes measurements along a single beam and one set of echo parameters can be measured at each range gate along the beam. Because more than one meteor echo might occur in each observation cell the transmitter pulse width and range gate separation were set to 15 km, and the first range gate was reduced to 120 km. Ideally,

this first range should be reduced even further, but a software limitation precluded this. The choice of a range separation of 15 km limited the maximum range to 1170 km. The integration time was also reduced from 7 s to 2 s, since meteor echoes have life times in the order of 0.5 s.

Figure 1 shows meteor echoes are evident as the GNREs at ranges less than about 700 km. There is a clear diurnal variation in echo occurrence, with very few echoes observed late in the afternoon (~17 LT). The top panel displays echo power, and it is apparent that the meteor echoes are generally weaker than the sea echoes observed via one-hop propagation at greater ranges. The leading edge of the sea scatter oscillates in range because of the passage of medium-scale gravity waves through the intervening region of ionospheric refraction. There is also a strong band of ionospheric echoes overlapping the meteor echoes at the beginning of the plot, and a tendency for bands of ionospheric echoes to expand equatorward at dusk and extend into the region of meteor echoes.

The middle panel of Figure 1 shows the LOS Doppler velocity of the radar echoes. Most of the echoes within the reduced range window of 1170 km shown in the figure have relatively low velocities and on the basis of velocity alone, meteor echoes do not stand out as a distinctly different population. In contrast, in the bottom panel showing the spectral widths, the meteor echoes are a mixture of echoes with low spectral width and unusually high spectral width. These characteristics will be examined further later.

A single beam campaign was run on 1 to 3 March 2003 to examine the dependency of meteor echo detection on the operating frequency of the radar. The radar was stepped through 18 licensed frequency bands between 9 and 20 MHz. The results are shown in Figure 2, which is a histogram of the number of meteor echoes per sounding, as a function of the start frequency of each band. These results are for the first 8 hours of the campaign when there was no evidence of contamination by ionospheric scatter. It is evident that the radar was most sensitive to meteors when operating at lower frequencies. The maximum occurrence rate was 10.0±0.4 echoes per 2 sec integration. The radar samples volumes determined by the beam width and pulse width at many ranges; hence numerous echoes can be detected per integration time. If it were not for small dead-time intervals between integrations, the peak occurrence rate implies it would be possible to achieve maximum detection rates >432,000 meteor echoes per day in the dawn sector.

The sensitivity of the radar to meteor echoes will depend on many factors, such as the frequency dependence of the scattering cross-section of meteors, and the variation of the radar antenna beam width which decreases with increasing frequency. The average backscatter power only decreased slightly with frequency, so we surmise that the decrease in occurrence rate with frequency was mostly due to the decreasing antenna beam width selecting a smaller volume of space, and thus fewer meteors. The decrease in the elevation angle of the main beam may also be a factor.

Conversely, the ratio of the antenna back- to forward lobes is larger at lower frequencies, making directional ambiguities a problem. The frequency 12 MHz was chosen for most of our campaigns because (1) it is an excellent working frequency for most night side ionospheric experiments, (2) it moderates the back lobe problem, (3) the echo detection rates are nevertheless satisfactory, and (4) the design of the radar was tuned for this frequency.

Specific examples comparing observations made at 12.05 MHz and 19.80 MHz are shown in Figure 3 where the number of meteor echoes, which occur at ranges less than ~700 km, is very much less at 19.80 MHz. At the time of these observations, the ionosphere favoured HF propagation at 12.05 MHz, so there is also significant ionospheric and sea scatter, mostly at ranges greater than the meteor echoes. However, there are excursions of direct half-hop ionospheric scatter into the meteor echo region from 21 to 06 hours and from 21 to 03 hours. At 19.80 MHz, the ionosphere did not favour one-hop propagation, so there were fewer sea echoes. However, half-hop ionospheric backscatter from the most intense irregularities persisted at the highest frequencies.

We call the bands of ionospheric scatter which descended in group range and merged into the meteor scatter "descending plasma streams" (DPSs). At further ranges (>1000 km) the ionospheric scatter probably emanated from 10-m scale F-region irregularities detected via half-hop propagation. However, the DPSs approached to within meteor echo ranges and probably represent scatter from irregularities located in the E-region and lower F-region. The DPSs commenced at dusk, and expanded equatorward in magnetic local time, implying they were echoes associated with proton aurora located at the equatorward edge of the auroral oval. Thus DPSs may be close relatives of the so-called "slow long-lived E-region plasma structures" (SLERPS) (Jayachandran et al., 2000).

All the echoes obtained for the campaign of 24 to 26 May 2003 at ranges less than 600 km were analysed to determine the characteristics of the echo population, and to examine criteria used to resolve the subset of meteor echoes. Figure 4 (a) shows histograms of the number of echoes versus the three main echo parameters, and Figure 4 (b) shows the corresponding histograms normalised to their most probable values. The histograms are also shown for echo populations selected using four different sets of criteria. The first population (black line) simply consists of all the echoes detected within ranges of 120 to 600 km, where 120 km was the first range for the campaign. The second population (green line) consists of echoes within the same range window, but with amplitudes of 3 to10 dB, and the third population (blue line) consists of echoes with high spectral width, viz. those with spectral widths 300 to 600 m s^{-1}. The final population consists of echoes with overall the most restrictive criteria applied (purple line). Again the same range window was considered, however, only echoes with powers, LOS velocities and spectral widths from 3 to 24 dB, ±50 m s^{-1}, and 0 to 50 m s^{-1} respectively, were considered. These criteria probably selected the meteor echoes giving the most accurate LOS velocities.

Some of the echoes probably do not represent backscatter from underdense meteors, and the relationship of their Doppler shift to the neutral wind is complicated. For example, the lower panels of the histograms clearly show a separate distribution of high spectral width echoes. These spectral widths are unusually large for meteor echoes, but they probably arise because the standard real-time analysis algorithm does not always give correct results for weak meteor echoes with modest signal-to-noise ratio. Moreover, the middle panel of Figure 4 (b) shows that the distributions of LOS velocity are equivalent for all four categories of echoes. This suggests that the different populations are dominated by meteor echoes, or perhaps other echoes from irregularities drifting with the neutral wind. Nevertheless, the unambiguous identification of underdense meteor echoes by their characteristic rapid rise and diffusive decay would improve the reliability of measurements.

Figure 5 shows plots of the neutral winds calculated for the 24 to 26 May campaign (cf. Fig. 1). First, the top panel (a) shows the total number of events detected every 15 minutes for separate echo populations following the criteria used in Figure 4. Note that one 16-beam scan was performed every minute, so the event rate per sounding is comparable to that shown in Figure 2. The large number of events accepted as meteor echoes easily permitted estimates of neutral winds using 15 minute bins, as opposed to the hourly bins used in previous studies. In fact, the large number of echoes detected enabled the analysis to be repeated using 1 minute bins, as shown in Figure 6 (to be discussed later). Figure 5 (b) shows the meridional wind (positive equatorward) and Figure 5 (c) the zonal wind (positive eastward) calculated for the separate echo populations. The black dots represent the unrestricted data, and the green stars the low powered echoes (3 to 10 dB). The blue triangles represent the echoes with unusually high spectral width (300 to 600 m s^{-1}), and the purple squares the meteor echoes identified using the most restrictive criteria.

The neutral winds were derived as follows. First, the horizontal component of the LOS Doppler velocities were calculated assuming that all meteor echoes had a reflection height of 95 km. This projection was performed at all ranges between 120 and 600 km and for all sixteen beams. Next the LOS horizontal components were averaged across all ranges but separately on all sixteen beams.

The standard errors were also calculated. The meridional winds (middle panel) were estimated by calculating the weighted average horizontal velocity on beams 7 and 8 because geographic south lies half-way between these two beams. In order to estimate the zonal wind (bottom panel), a beam-swinging algorithm was applied if horizontal components were available on at least 5 beams. The best-fit curve to the horizontal velocities on all sixteen beams was constrained by the aforementioned estimate of the meridional wind, as well as the corresponding standard errors.

The estimate of the meridional wind assumed homogeneous meridional flow across beams 7 and 8 and all ranges between 120 and 600 km, whereas the estimate of the zonal wind assumed homogenous meridional and zonal flow across all 16 beams and the same ranges. The estimates of both components assumed the homogeneous flows had zero vertical wind, and the wind was stationary for 15-minute intervals. The estimates of the meridional wind (middle) show less scatter and are more accurate because they were closer to a direct measurement. However, because of all the assumptions made, both high time resolution wind components are considered "synoptic" in spatial scale.

As expected, the scatter in the estimated winds increased (decreased) at dusk (dawn) when the number of available echoes was a minimum (maximum). However, the scatter was greatest of all for the echoes with unusually large spectral widths (blue triangles), suggesting that these were actually meteor echoes with less accurate LOS velocity and very poorly determined spectral width. Nevertheless, there is consistency in the wind values derived from each of the echo populations, and they all provided a consistent synopsis of the winds in the MLT region just south of Tasmania. The net wind direction throughout the campaign was poleward and westward, though becoming more equatorward towards the end of the campaign, and there were clear variations on gravity-wave and tidal time scales.

The large number of meteor echoes detected every 15 minutes enabled a higher time resolution analysis. One full scan lasting 32 s was completed every minute during the 24 to 26 May campaign, so here we calculate the neutral winds by using 1-minute time bins, the maximum time resolution permitted by the data. Figure 6 (a) shows the total number of events per minute for all the echoes with power >3 dB detected within ranges 120 to 600 km during the time interval 21 LT, 25 May to 10 LT, 26 May 2003. Strictly, the use of more stringent selection criteria is recommended, but an examination of Figure 1 reveals that meteor echoes were dominant, except possibly for a few isolated patches of E-region scatter. Hundreds of events were observed per minute, with a major peak around dawn, and with evidence for localised bursts in meteor activity.

Figure 6 (b) and (c) show the meridional and zonal winds, respectively. The error bars suggest the extent to which the scatter in the data is caused by "measurement noise," but there is clear evidence for greater variability than revealed in Figure 5. For example, genuine wind "gusts" reoccurred on gravity-wave time scales (2 to 4 hours), and are better resolved and surge to much larger values than shown in Figure 5. These results illustrate the potential of the TIGER radar to measure mesospheric neutral winds at short time scales (<1 minute). The geophysical significance of these winds combined with a model comparison will be the focus of a separate study.

3. Recommendations

In order to optimise the detection rate of meteor echoes, we recommend the use of transmitter pulses of width 15 km and range gates separated by 15 km commencing at ranges of ~60 km. The use of shorter range sampling will also facilitate better resolution of the height variation of the winds. The integration time should also be reduced to 2 s or less. These are not the standard operating parameters used for ionospheric research, but they result in the detection of numerous meteor echoes permitting the calculation of neutral winds with greater accuracy and time resolution since they help to constrain the results of the beam steering algorithm.

Work continues on resolving directional ambiguities in the detection of meteor echoes due to the presence of back lobes (S. Yukimatu, private communication). We recommend the use of a radar operating frequency of ~12 MHz, and even lower when the back lobe ambiguities can be resolved. The latter will permit the measurement of neutral winds in two separate MLT regions displaced several hundred kilometres north and south of a radar pointing in the meridional direction, and so provide at least an estimate of the meridional gradient.

Our analysis shows that the criteria used to identify meteor echoes are not critical for estimating the synoptic-scale meteor winds. The present approach will remain valid for the derivation of MLT winds, and especially for the re-processing of SuperDARN data archives which now extend back ~20 years. However, it will be superseded by the use of a new radar operating system which permits the direct detection of the rise and decay of meteor echoes (Yukimatu and Tsutsumi, 2003), combined with the use of improved signal processing (Yukimatu et al., 2002) and new digital receivers. This will facilitate better horizontal and vertical resolution of the MLT winds. Further investigations should involve a comparison of neutral winds detected using the present method and the classical implementation of Yukimatu and Tsutsumi (2003).

Finally, the "descending plasma streams" (DPS) which merged into and disappeared at the group ranges of meteor echoes were clearly echoes from the auroral ionosphere. Their behaviour resembled sporadic E associated with proton aurora as observed by other SuperDARN radars, and are a phenomenon requiring further investigation.

4. Acknowledgments

This work was supported by the Australian Research Council, the Australian Antarctic Science Advisory Committee, and the TIGER Consortium Partners (http://www.tiger.latrobe.edu.au/). We thank Sessai Yukimatu-san for providing us with access to his new TMS radar operating system, and Harvey Ye for his help in the design and operation of our experiments.

5. References

Arnold, N.F., Robinson, T.R., Lester, M., et al. Super Dual Auroral Radar Network observations of fluctuations in the spectral distribution of near range meteor echoes in the upper mesosphere and lower thermosphere. Ann. Geophys. 19, 425–434, 2001.

Arnold, N.F., Cook, P.A., Robinson, T.R., et al. Comparison of F-region Doppler drift winds measured by the SuperDARN Finland HF radar over an annual cycle using the Kiruna VHF meteor radar. Ann. Geophys. 21, 2073–2082, 2003.

Dyson, P. L., Devlin, J. C. The Tasman International Geospace Environment Radar. The Physicist (AIP). 37, 48–53, 2000.

Greenwald, R.A., Baker, K.B., Dudeney, J.R., et al. DARN/SuperDARN: A global view of the dynamics of high latitude convection. Space Sci. Rev. 71, 761–796, 1995.

Hall, G.E., MacDougall, J.W., Moorcroft, D.R., et al. Super Dual Auroral Radar Network observations of meteor echoes. J. Geophys. Res. 102, A7, 14603–14614, 1997.

Hussey, G.C., Meek, C.E., André, D. et al. A comparison of Northern Hemisphere winds using SuperDARN meteor trial and MF radar wind measurements. J. Geophys. Res. 105(D14), 18053–18066, 2000.

Jayachandran, P.T., St.-Maurice, J.-P., MacDougall, J.W., Moorcroft, D.R. HF detection of slow long-lived E region plasma structures. J. Geophys Res. 105(A2), 2425–2442, 2000.

Jenkins, B., Jarvis, M.J. Mesospheric winds derived from SuperDARN HF radar meteor echoes at Halley, Antarctica. Earth Planets Space. 51, 685–689, 1999.

MacDougall, J.W., Li, X. Meteor observations with a modern digital ionosonde. J. Atm. Solar-Terr. Phys. 63, 135–141, 2001.

Viereck, R.A. A review of mesospheric dynamics and chemistry. Rev. Geophys. 29, 1132–1142. 1991.

Yukimatu, A.S., Tsutsumi, M. A new SuperDARN meteor wind measurement: Raw time series analysis method and its application to mesopause region dynamics. Geophys. Res. Lett. 30 (1), 1026, doi: 10 1029/2002Gl016560, 2003.

Yukimatu, A.S., Tsutsumi, M., Yamagishi, H., Sato, N. 2002. A new method for monitoring and removing SuperDARN radar DC offsets. Adv. Pol. Upp Atm. Res. 16, 181–192, 2002.

Table 1.

Characteristic	Nominal Values
Power	3–24 dB
LOS Doppler velocity	± 40 m s^{-1}
Spectral width	>1 and <50 m s^{-1}
Elevation angle	N/A °
Altitude	90–110 km
Range	<500 km

Figure Captions

Fig. 1. Summary plots of the three main echo parameters recorded using frequency 12,050 kHz and beam 7 during 00 hours LT, 24 May to 08 LT, 26 May 2003 (LT=UT+10 hours). The top panel shows the backscatter power (dB), the middle panel the LOS Doppler velocity (m s^{-1}), and the bottom panel the Doppler spectral width (m s^{-1}), all versus group range and time. The parameter values are determined by the colour scales at right, and the two thin, horizontal lines indicate the ranges corresponding to magnetic latitudes of −60° and −65°.

Fig. 2. A histogram showing the number of meteor echoes detected per 2-s integration on beam 7 versus the starting transmission frequency of each licensed band during 10 to 18 LT, 1 March 2003.

Fig. 3. Summary plots of echoes recorded on beam 7 during 10 LT, 1 March to 10 LT, 3 March 2003 using **(a)** transmission frequency 12,050 kHz, and **(b)** transmission frequency 19,800 kHz.

Fig. 4. (a) Histograms of the number of echoes recorded between ranges 120 to 600 km for **(i)** the backscatter power (dB), **(ii)** LOS Doppler velocity (m s^{-1}), and **(iii)** Doppler spectral width (m s^{-1}). As explained in the text, the black line represents the unrestricted echoes, the green line the echoes with powers of 3 to 10 dB, the blue line the echoes with unusually large spectral width (300 to 600 m s^{-1}), and the purple line the meteor echoes identified using the most restrictive criteria. **(b)** The same as part (a) except the occurrence histograms have been normalised to their most probable values.

Fig. 5. (a) The number of meteor echoes detected during each 15 minute interval during 00 LT, 24 May to 08 LT, 26 May 2003. The results are shown using the four different set of criteria used in Figure 4. **(b)** The corresponding meridional winds calculated using the Doppler shifts observed on beams 7 and 8. A positive wind indicates equatorward (northward) motion. **(c)** The zonal winds calculated using the beam-swinging technique described in the text. A positive wind indicates eastward motion.

Fig. 6. **(a)** The number of meteor echoes detected during each 1 minute interval during 21 LT, 25 May to 10 LT, 26 May 2003. The results are shown using all the echoes with power >3 dB detected within the ranges 120 to 600 km. **(b)** The corresponding meridional and **(c)** zonal winds calculated in the same way as the results shown in Figure 5, except using smaller time intervals.

First, we thank both referees for their constructive, helpful comments shown in bold.

Reply to Reviewer 1

I don't agree with the tendency of the text to define all such data as meteor trail echoes. The feature which really distinguishes a meteor trail is the quick rise time and exponential decay. Neither of these parameters is (directly) available in the present TIGER data. It would be interesting to compare results from the present type of analysis with the newer SuperDARN systems being developed to select and measure trails from signal vs. time directly. One additional criterion - viz. selection of isolated (in time and beam) echoes would increase the probability of their being from a meteor trails (but at a significant loss in numbers of echoes).

Currently TIGER is unable to detect the rise and decay of meteor echoes; however in the recommendations we have discussed the new radar operating system which will permit such detections, and acknowledge the need to make the recommended comparison.

Pg. 3 para. 2: Why would higher transmitted frequencies have fewer echoes ... is the S/N lower because of the fixed 2s integration and expected shorter trail duration? Does the variation seen with frequency support that argument?

The sensitivity of the radar to meteor echoes will depend on many factors, such as the frequency dependence of the scattering cross-section of meteors, and the variation of the radar antenna beam width which decreases with increasing frequency. Higher transmission frequencies produce a smaller antenna beam width, therefore a smaller volume of space is sampled and fewer meteor echoes are detected. The decrease in the elevation angle of the main beam may also be a factor at high frequencies. Figure 2, a histogram of the number of meteor echoes as a function of the start frequency of each band supports this.

Pg 3, para 2: How can there be more than 1 trail per integration?

During a 2-s integration period the radar beam width and pulse width selects a substantial volume of space, therefore numerous meteor echoes could occur in a given integration time.

Pg. 4 Para 5: This plot shows a maximum of 60 echoes in 15 min. How is this reconciled with the 10 trails / 2 sec mentioned on page 3 para 2.

Thank you very much for pointing out this obvious mistake. We identified a bug in our beam-swinging algorithm which effectively discarded numerous echoes. As a consequence, Figure 5 now shows a reconcilable number of events per 15 minute bin, and

we now include Figure 6 to illustrate the potential for SuperDARN to achieve high time resolution neutral wind measurements.

Pg. 4 Para. 2 - the comment that maybe the echoes are not trails but "seem to be drifting with the same velocity" and so they give the correct wind is not acceptable. Meteor trails have a simple mechanism related to the neutral wind that can be used to explain echo Doppler velocities; other types of scattering may not be as simple to relate to wind speed. The comment should be qualified a little more.

This comment has been removed and the text has been revised to better explain the difficulties. For example, now we state that "Some of the echoes probably do not represent backscatter from under dense meteors, and the relationship of their Doppler shift to the neutral wind is complicated." As suggested by the referee, we also point out that "the unambiguous identification of under dense meteor echoes by their characteristic rapid rise and diffusive decay would improve the reliability of measurements."

Pg 3 1st para: Why is 3-24dB considered more restrictive than the 3-10dB alternate data selection criteria mentioned in the last para. on pg. 3

Overall, more restrictions were applied to the 3-24 dB data set, rather than the 3-10 db data set for which only power was restricted. The text has been reworded to make this point clearer.

Figure 4a,b :colour or not - these histograms are hard to read, mostly because they are "square", which puts vertical lines directly on top of each other. Shifting the histograms laterally a small amount with respect to each other or just doing straight line plots between the top-centres of the bins would help separate the different categories.

The curves in the top panels have been replaced by bar-chart style line plots because they were the most difficult to separate. In subsequent panels, each data set is now represented by a coloured solid line, making them much clearer to separate.

Pg 1 MacDougall et al., reference list says 2000

The MacDougall reference has been corrected.

Pg 4. 1st and 3rd para: The spectral width is quoted in m/s; does this refer to radial speed of the scatterers (i.e. 1/2 the Doppler velocity) or is it just Doppler frequency times wavelength?

We have included a sentence in "Observations and Analysis" defining spectral width: "The spectral widths are a measure of the spread of LOS Doppler velocity in the sampling volume which is determined but the beam width and pulse width."

Pg 4., 2nd para: nitpick: These are not probability plots, they are occurrence histograms normalized to their most probable value.

We now refer to the plots as "occurrence histograms".

Reference list: Yukimatu 2003 not referred to in text.

Yukimatu 2003 in an important reference and we now cite it in the text.

Fig 1. add time conversion to caption:"LT = UT +/- ... "

UT to LT conversions have been added to the caption.

There is a spurious unlabelled table included (pg. 8) - it looks to be data for Figure 2.

Table 1 is not spurious. We referred to it in the introduction.

Thank you for your numerous constructive comments.

Reply to Reviewer 2

Abstract: the abstract does not summarise the results of the paper. Since the title is about "optimising winds" the abstract needs to say how this is achieved. Since you feel optimizing meteor echo rate is equivalent to optimizing wind observations, adding a sentence or two stating the conventional SuperDARN operational parameters, together with the recommended parameters (first sentence of Recommendations section), will be sufficient. Incidentally, the last paragraph of this section may be a better summary of the descending plasma streams, which will now be more easily identified and therefore less likely to contaminate results. Could you re-work the abstract so that it becomes a succinct summary of the results in the paper.

The abstract has been reworked to include the conventional SuperDARN operating parameters as well as some of our "optimized" parameters. The abstract has also been

reworked to better summarise our results and give an overview of the contents of the paper.

The Figure captions for Figures 1, 3 and 5 are awkward to follow and inaccurate. In Figure 1 the start time is 12 UT, in the Figure caption, while the plot starts at hour 0. This means the axis caption should just read HOURS. Since local time features in your discussion of the results, the figures will all be more functional, conveying their information more quickly, if the UT start is the start hour of the data series, and if a local time axis is also added to the Figures. It is also unhelpful that there is no roll-over to 00 UT after 24 hours. In fact, given the nature of your discussions, probably it would be better to change all time references to Local Time, since the key discussion point about meteor fluxes is their strong local-time diurnal variation.

The figures have been revised to display Local Time, and indicate the roll-over to 00 LT for a new day. The figure captions have also been revised to make them easier to understand.

The histograms in Figures 4(i-a) and 4(i-b) are difficult to follow when different lines merge. Since the bin size is reasonable large, can you try interlacing (some plotting packages do this automatically). Maybe try different line thicknesses. I appreciate the effort to use both colour and line-type, but it still doesn't work. You need to do something to make the histograms easier to identify when they merge. It is made even harder because the plot does not show the top of the distributions.

The curves in the top panels have been replaced by bar-chart style line plots because they were the most difficult to separate. In subsequent panels, each data set is now represented by a coloured solid line, making them much clearer to separate.

References: MacDougall et. Al. is 2001 in the text and 2000 in the reference list. Could you correct this please. Also, I could not find Yukimatu et. al. 2003 in the text although it is the reference list.

Both references have been corrected.

It is possible to calculate the minimum line density of trails detected by SuperDARN radars (e.g., McKinley)? This is a useful meteor radar parameter and is an indication of the type of returns being observed. You can then say whether under- or over-dense meteors dominate the meteor populations being observed. This is useful because over-dense meteor trails can persist for a long time producing multiple reflection points, possibly in the same range-bin. I don't know whether this is likely to produce errors in wind estimates or not.

The work of Yukimatu and Tsutsumi (2003) demonstrates that the meteor echo population is dominated by under-dense meteor echoes, but over-dense meteor echoes, and E-region backscatter also occurs.

Is it worth comparing these "synoptic estimates" of winds with wind models? Also, I was unsure whether "greater accuracy and time resolution" was relevant at a synoptic level centred on 95 km?

As we now point out in the text, a comparison between our neutral wind results and wind models would be very beneficial. However, this task is beyond the scope of our initial explorative study. The referee's point about "synoptic estimates" is taken, and the text has been revised. The winds are certainly synoptic in space, but it is also important to demonstrate the capability of the radars to make high time resolution neutral wind measurements.

Thank you for your numerous constructive comments.

Figure1Colour

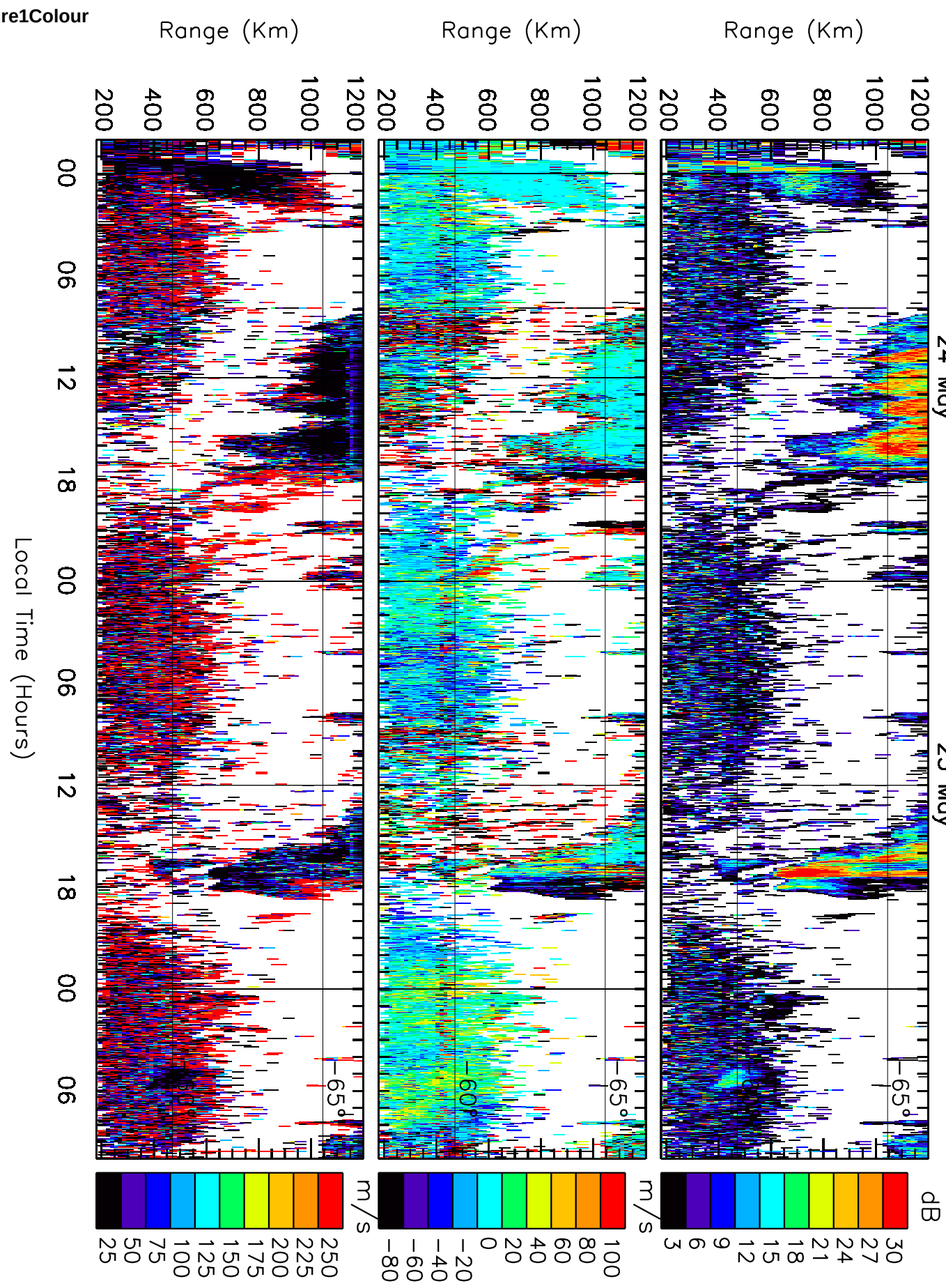

Figure2

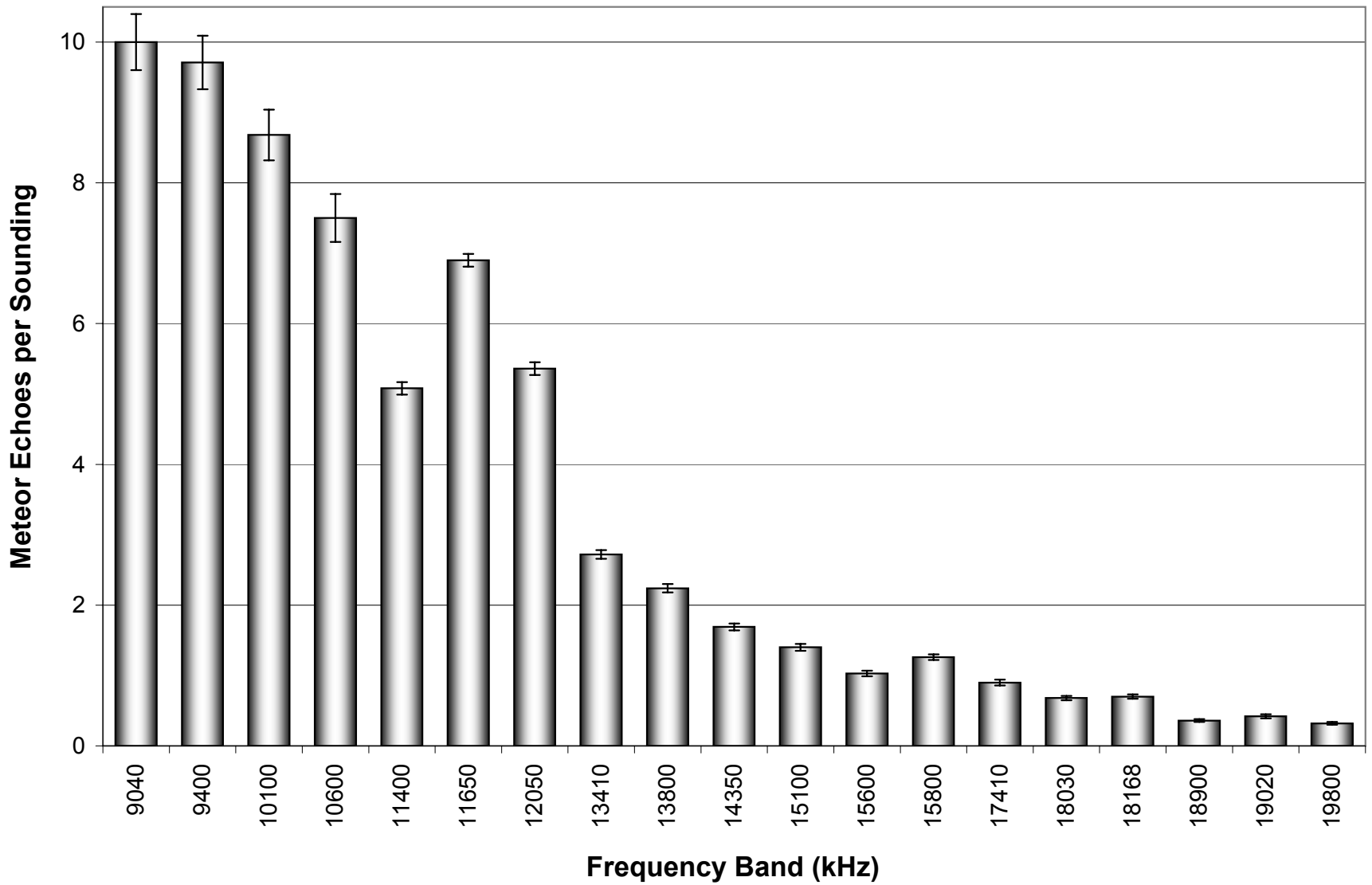
Meteor Echoes per Sounding
0
2
4
6
8
10
9040
9400
10100
10600
11400
11650
12050
13410
13800
14350
15100
15600
15800
17410
18030
18168
18900
19020
19800
Frequency Band (kHz)

Figure3aColour

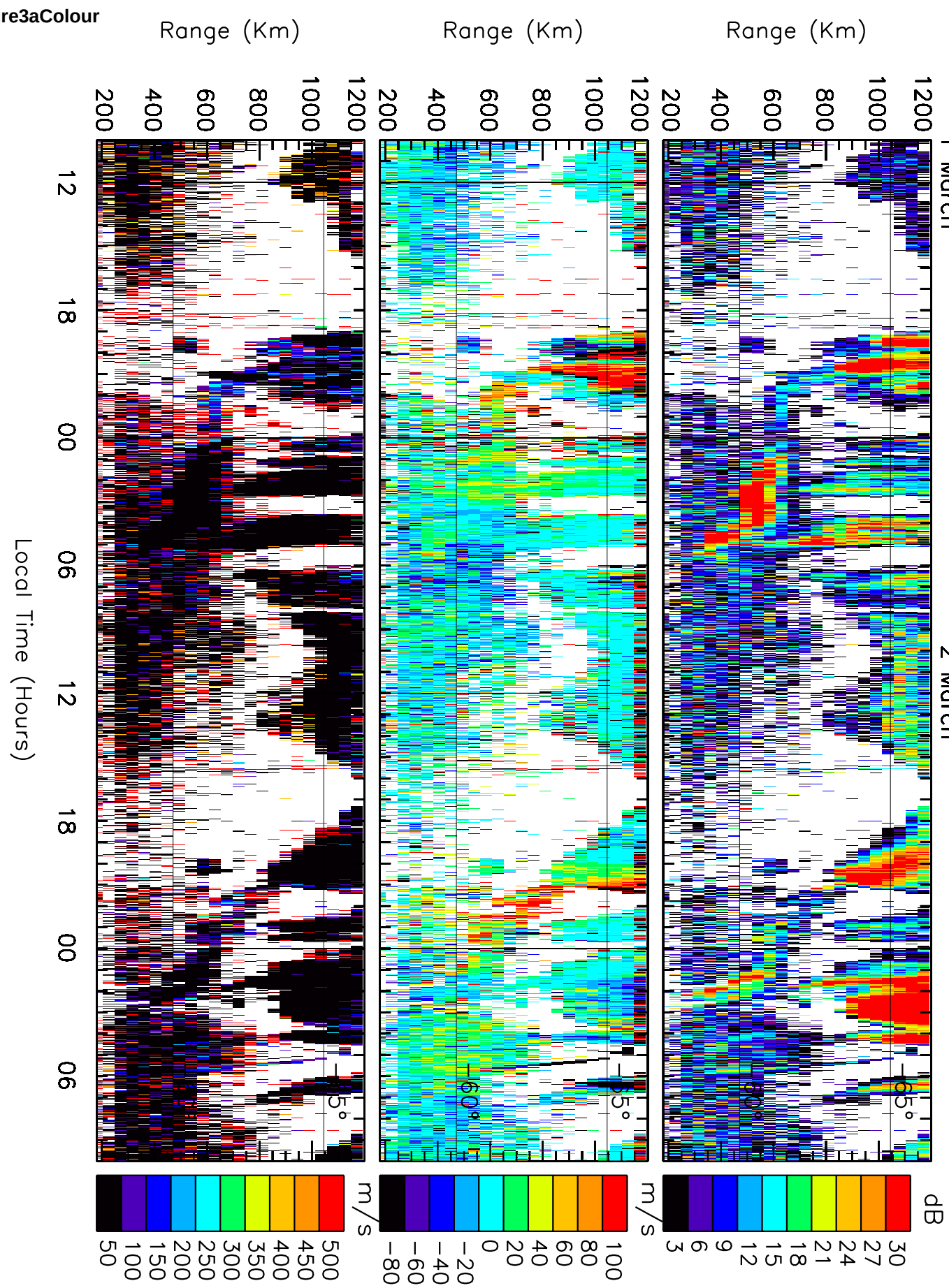

Figure3bColour

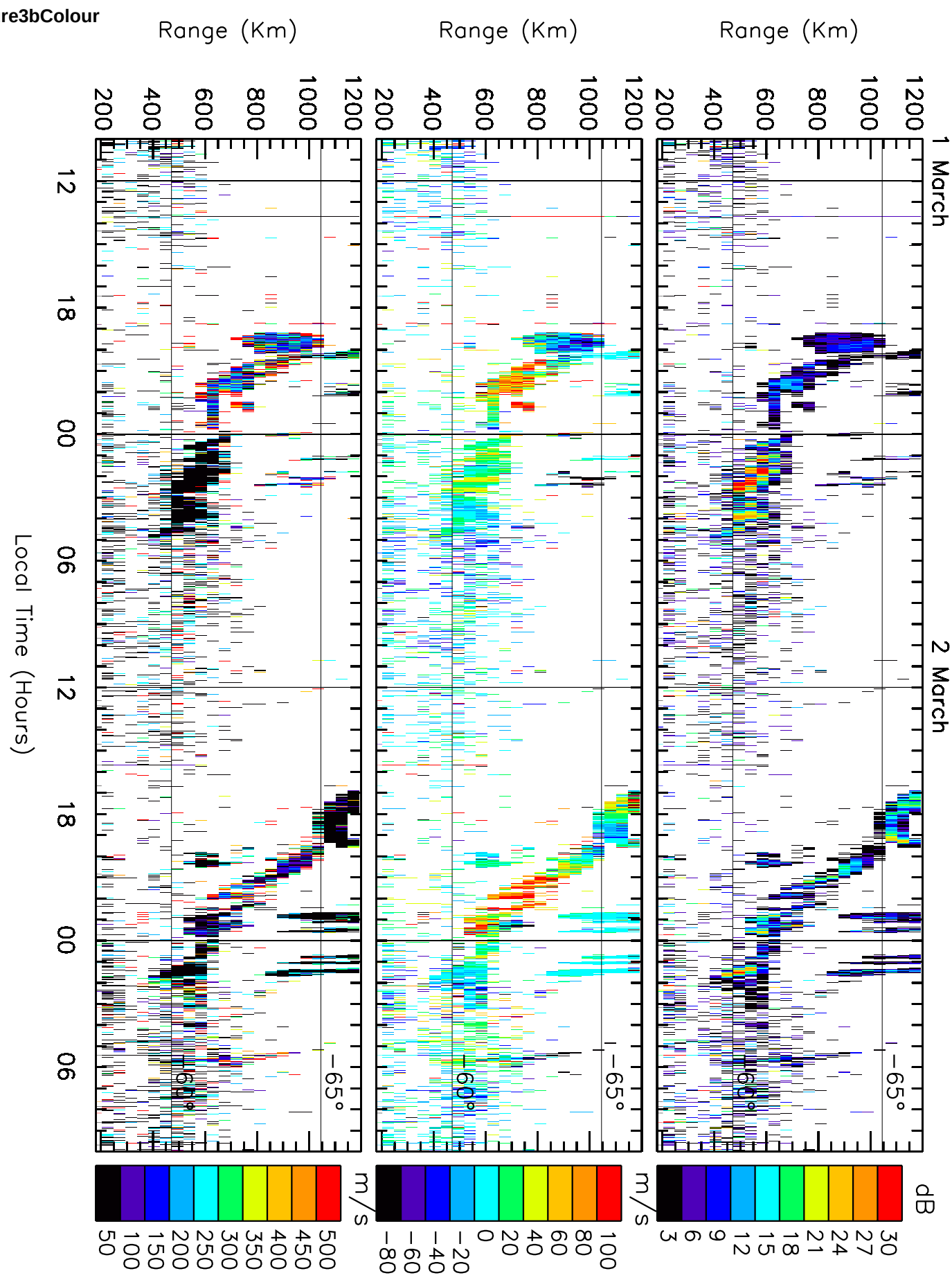

Figure4aColour

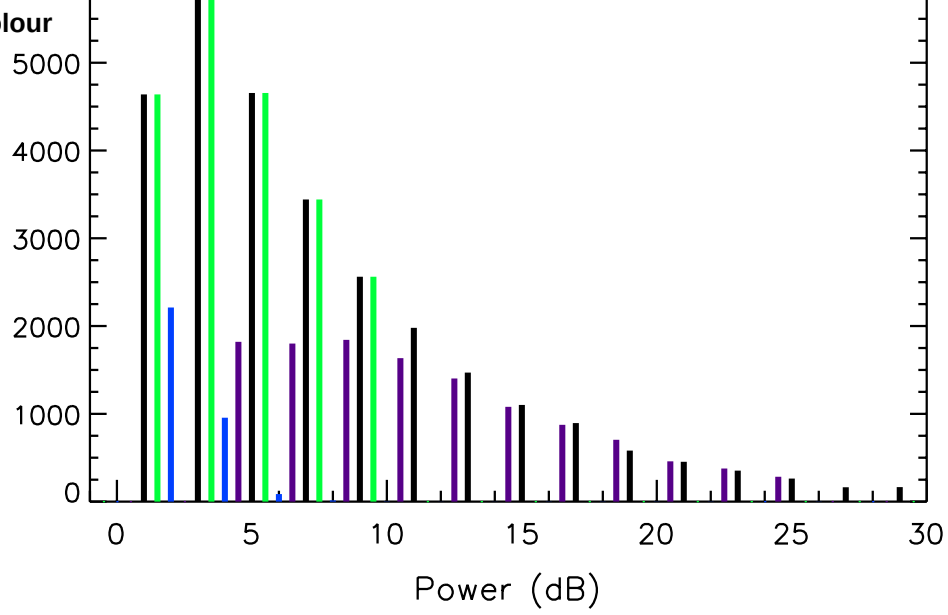

(i)

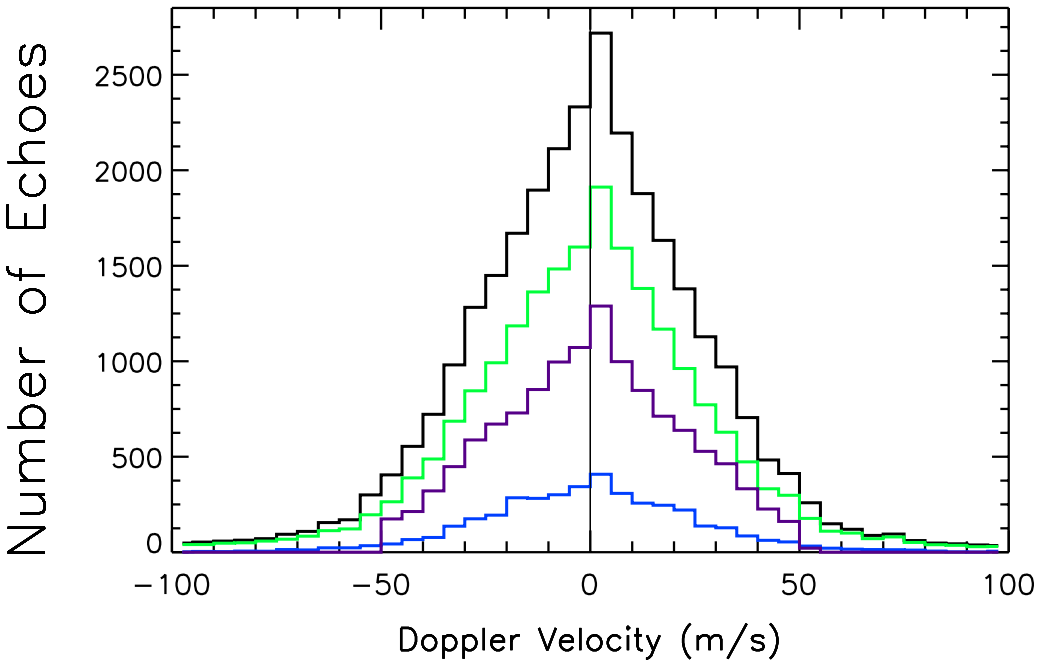

(ii)

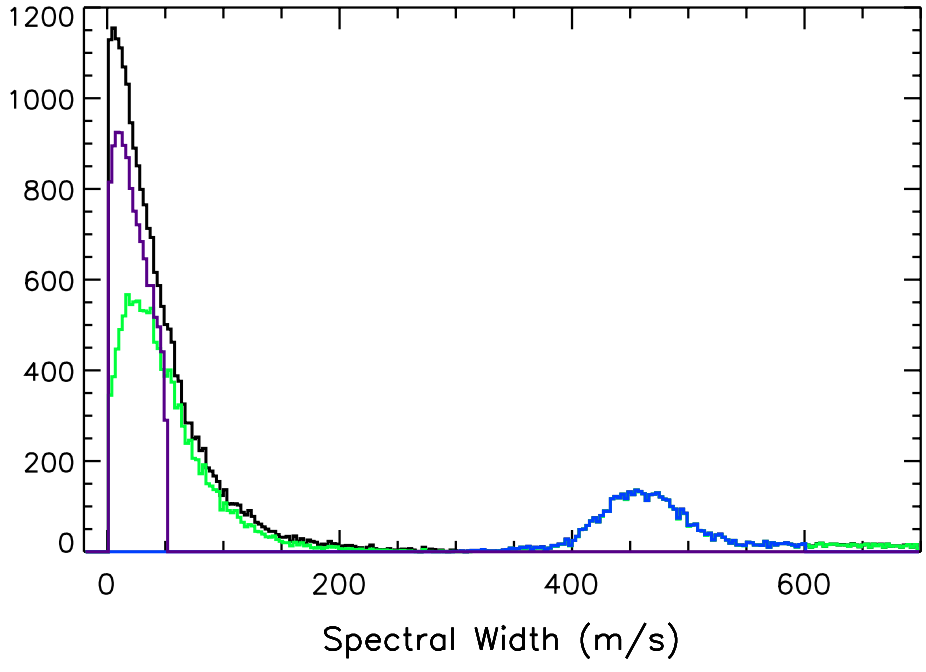

(iii)

Figure4bColour

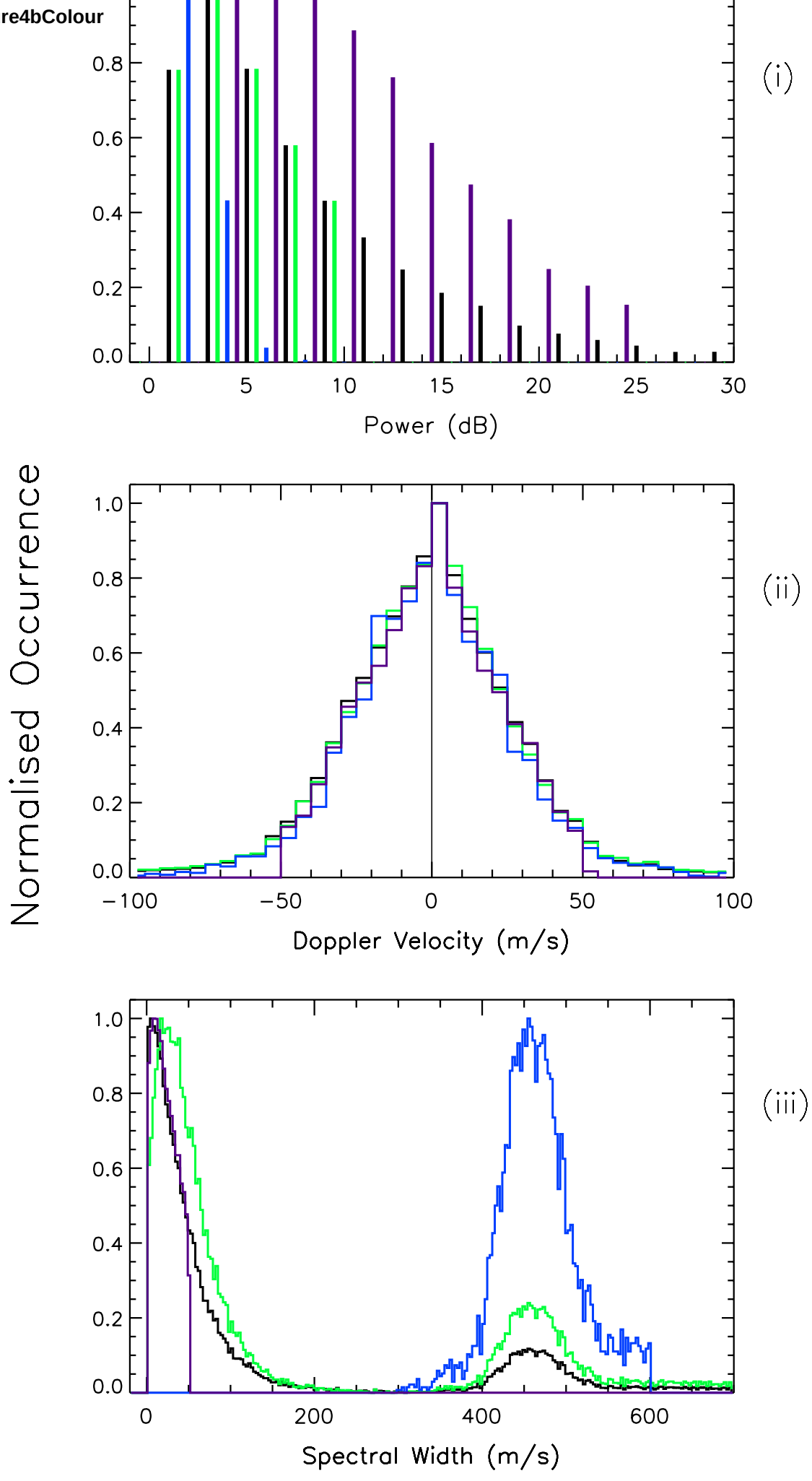

Figure5Colour

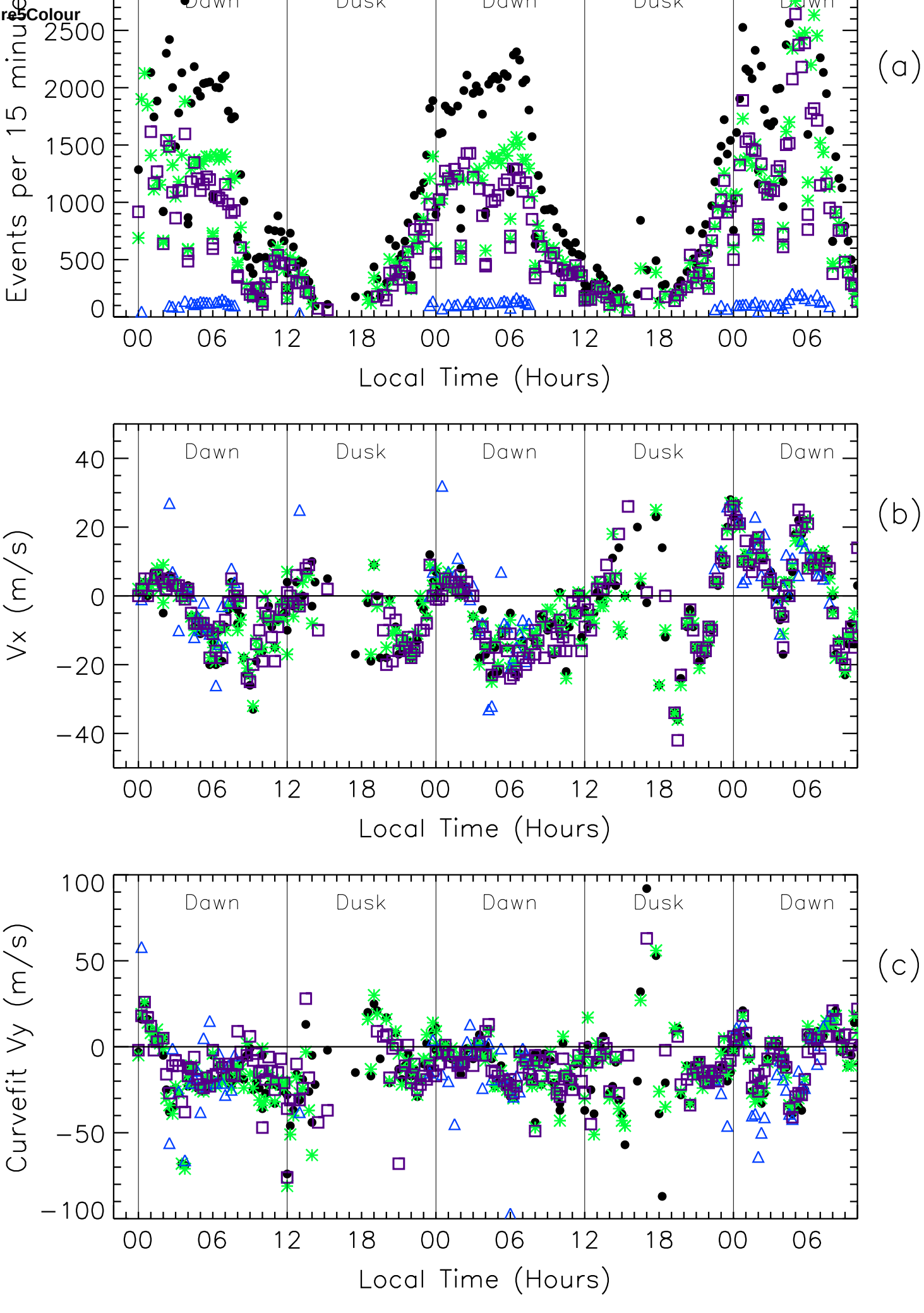

Figure6

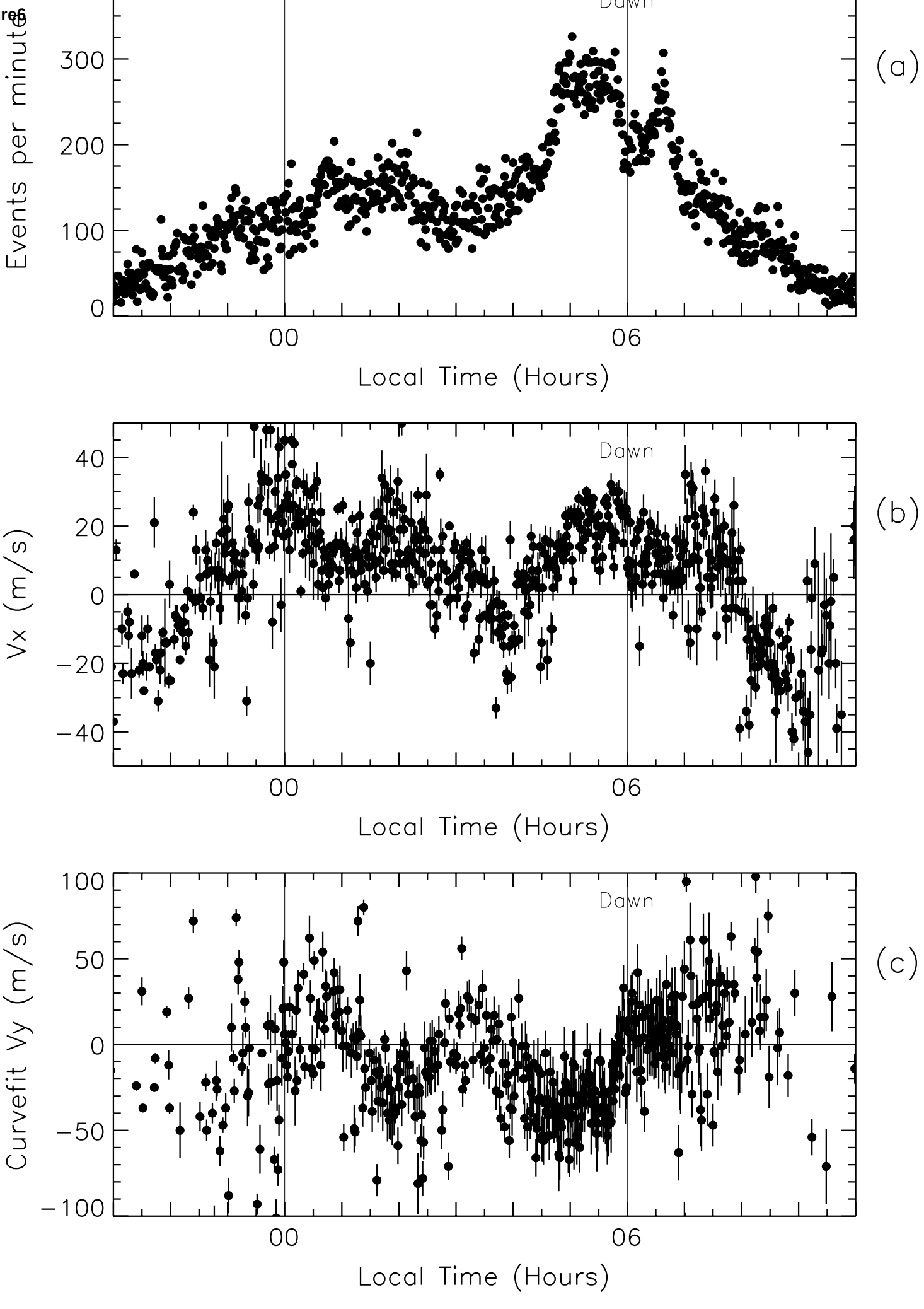
Dawn
Events per minute
0
100
200
300
00
06
Local Time (Hours)
(a)
Dawn
Vx (m/s)
40
20
0
−20
−40
00
06
Local Time (Hours)
(b)
Dawn
Curvefit Vy (m/s)
100
50
0
−50
−100
00
06
Local Time (Hours)
(c)

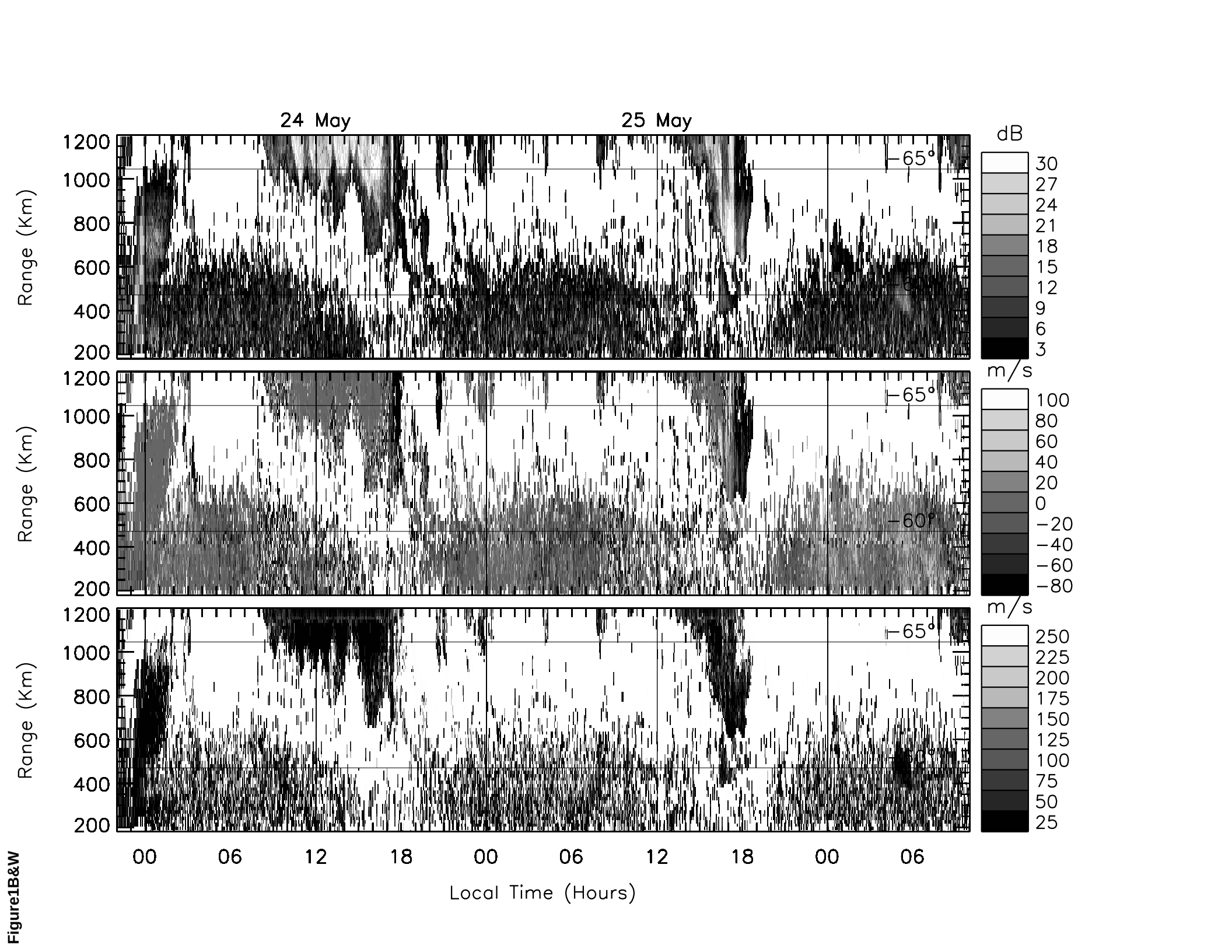
24 May
25 May
Range (Km)
1200
1000
800
600
400
200
−65°
dB
30
27
24
21
18
15
12
9
6
3
−60°
m/s
100
80
60
40
20
0
−20
−40
−60
−80
250
225
200
175
150
125
100
75
50
25
00
06
12
18
Local Time (Hours)

Figure1B&W

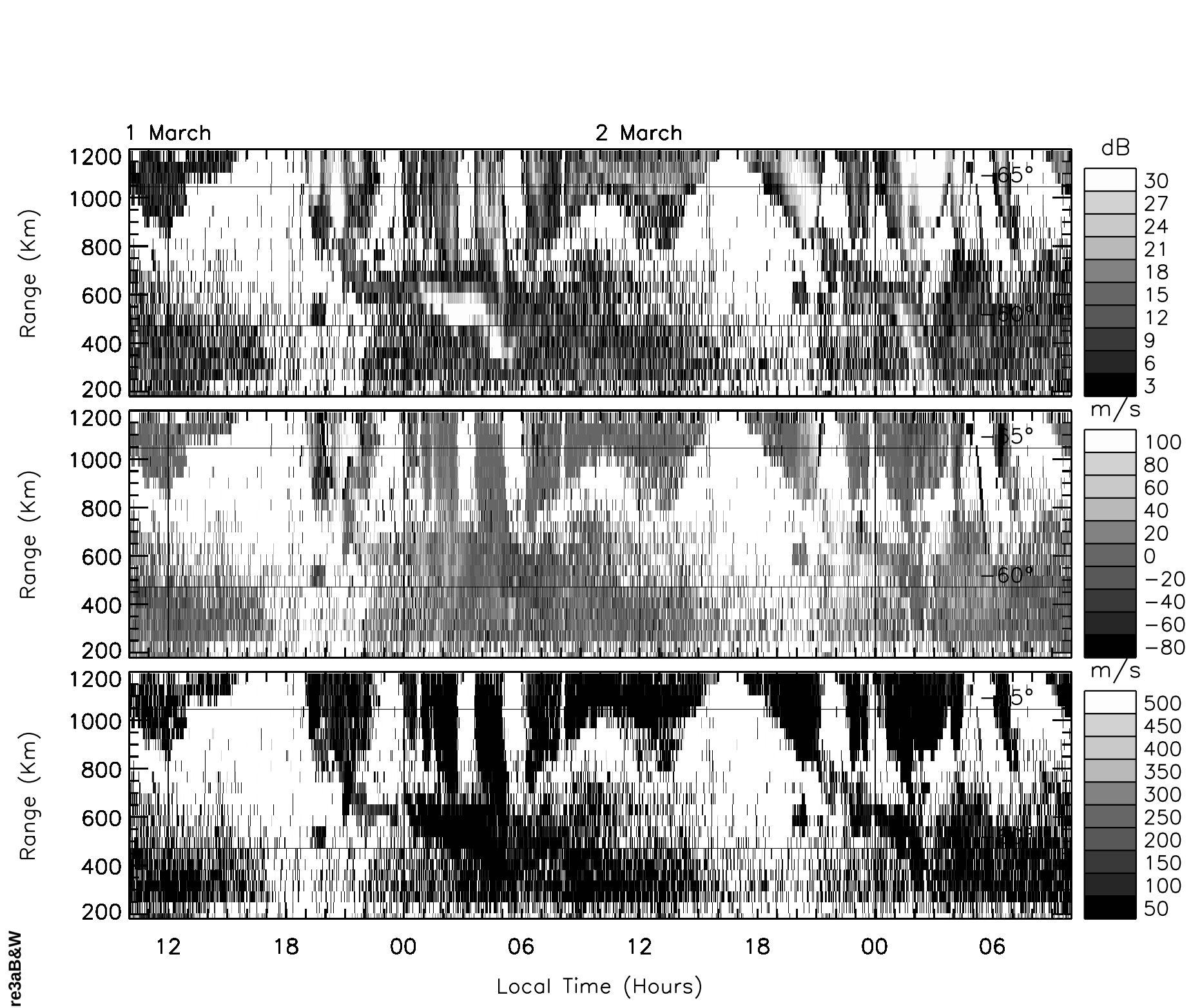
1 March
2 March
Range (Km)
1200
1000
800
600
400
200
−65°
−60°
−55°
dB
30
27
24
21
18
15
12
9
6
3
m/s
100
80
60
40
20
0
−20
−40
−60
−80
500
450
400
350
300
250
200
150
100
50
12
18
00
06
Local Time (Hours)

Figure3aB&W

Figure3bB&W

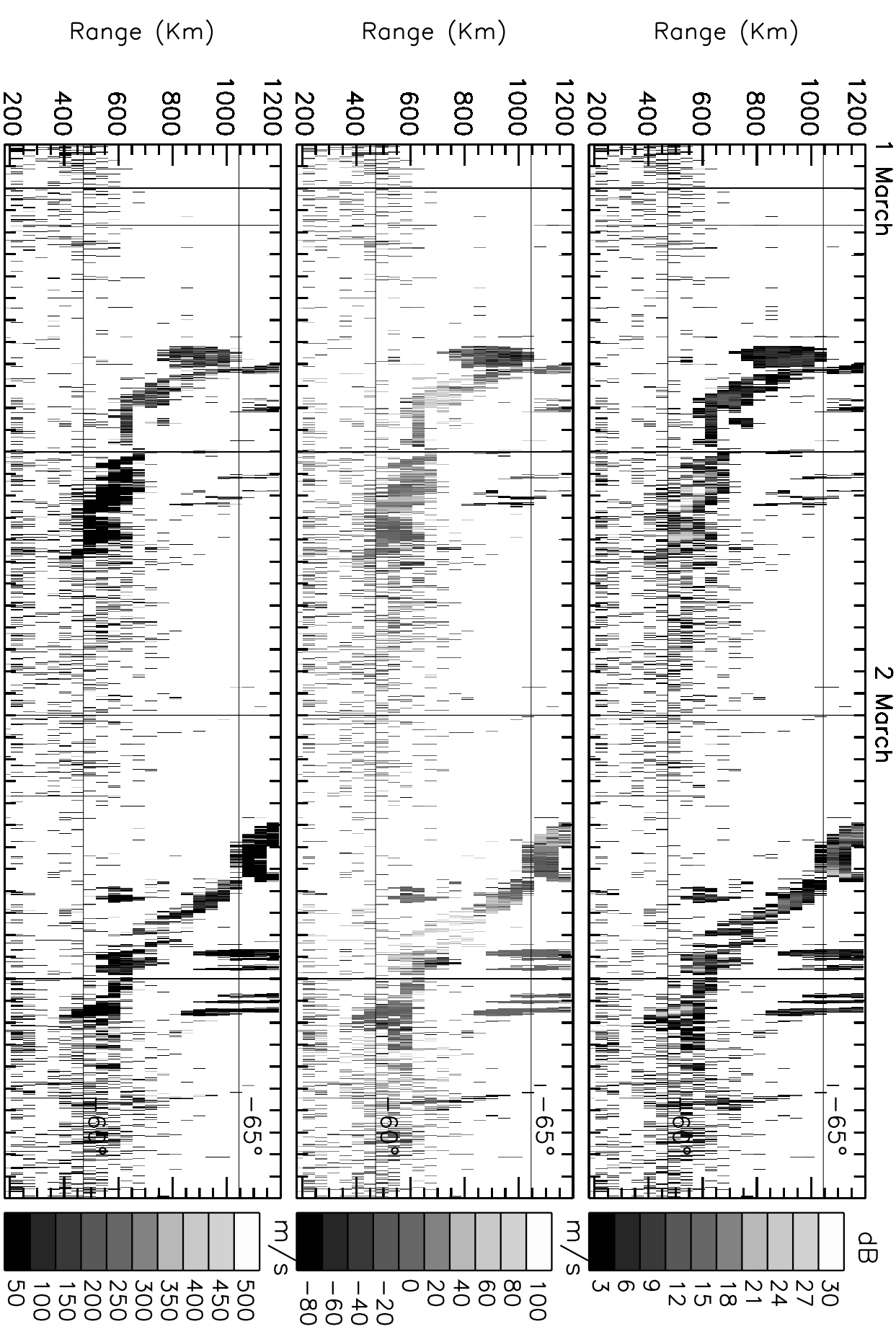
Range (Km)
Range (Km)
Range (Km)
200
400
600
800
1000
1200
1 March
2 March
−65°
−60°
−65°
−60°
−65°
−60°
dB
3
6
9
12
15
18
21
24
27
30
m/s
100
80
60
40
20
0
−20
−40
−60
−80
m/s
50
100
150
200
250
300
350
400
450
500
12
18
00
06
12
18
00
06
Local Time (Hours)

Figure4aB&W

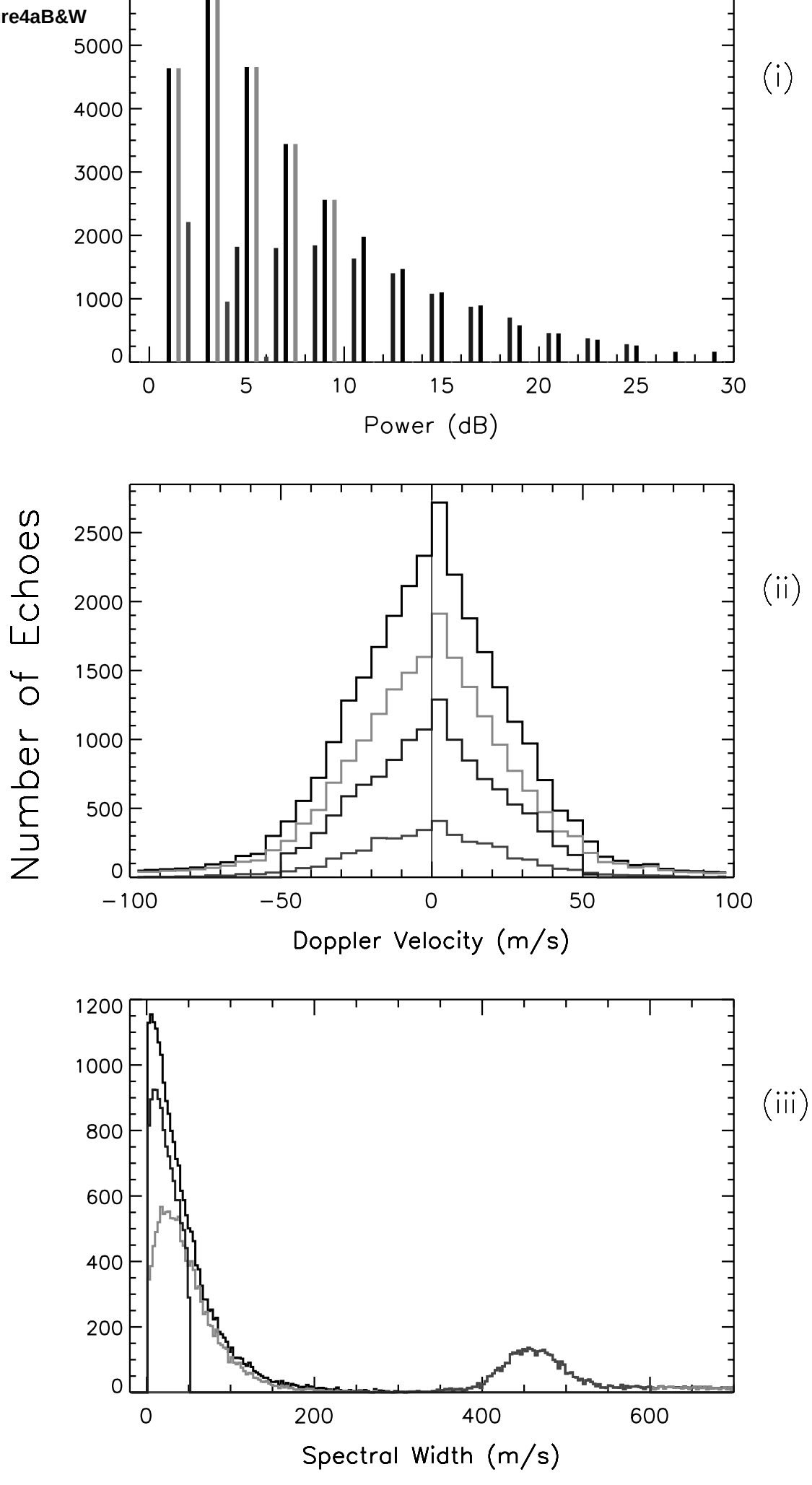
5000
4000
3000
2000
1000
0
0
5
10
15
20
25
30
Power (dB)
(i)
Number of Echoes
2500
2000
1500
1000
500
0
−100
−50
0
50
100
Doppler Velocity (m/s)
(ii)
1200
1000
800
600
400
200
0
0
200
400
600
Spectral Width (m/s)
(iii)

Figure4bB&W

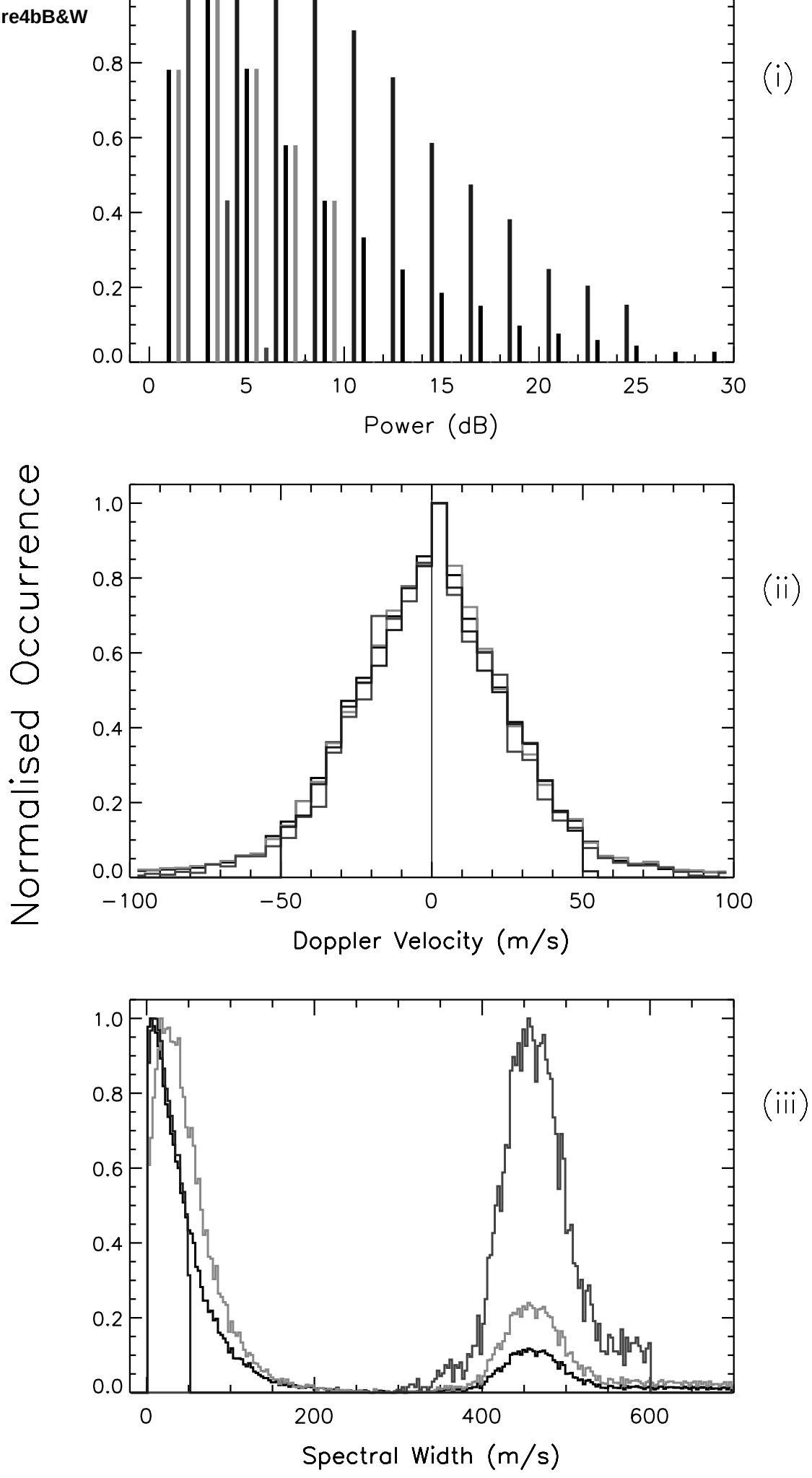
(i)
0.0
0.2
0.4
0.6
0.8
0
5
10
15
20
25
30
Power (dB)
Normalised Occurrence
(ii)
1.0
0.8
0.6
0.4
0.2
0.0
−100
−50
0
50
100
Doppler Velocity (m/s)
(iii)
1.0
0.8
0.6
0.4
0.2
0.0
0
200
400
600
Spectral Width (m/s)

Figure5B&W

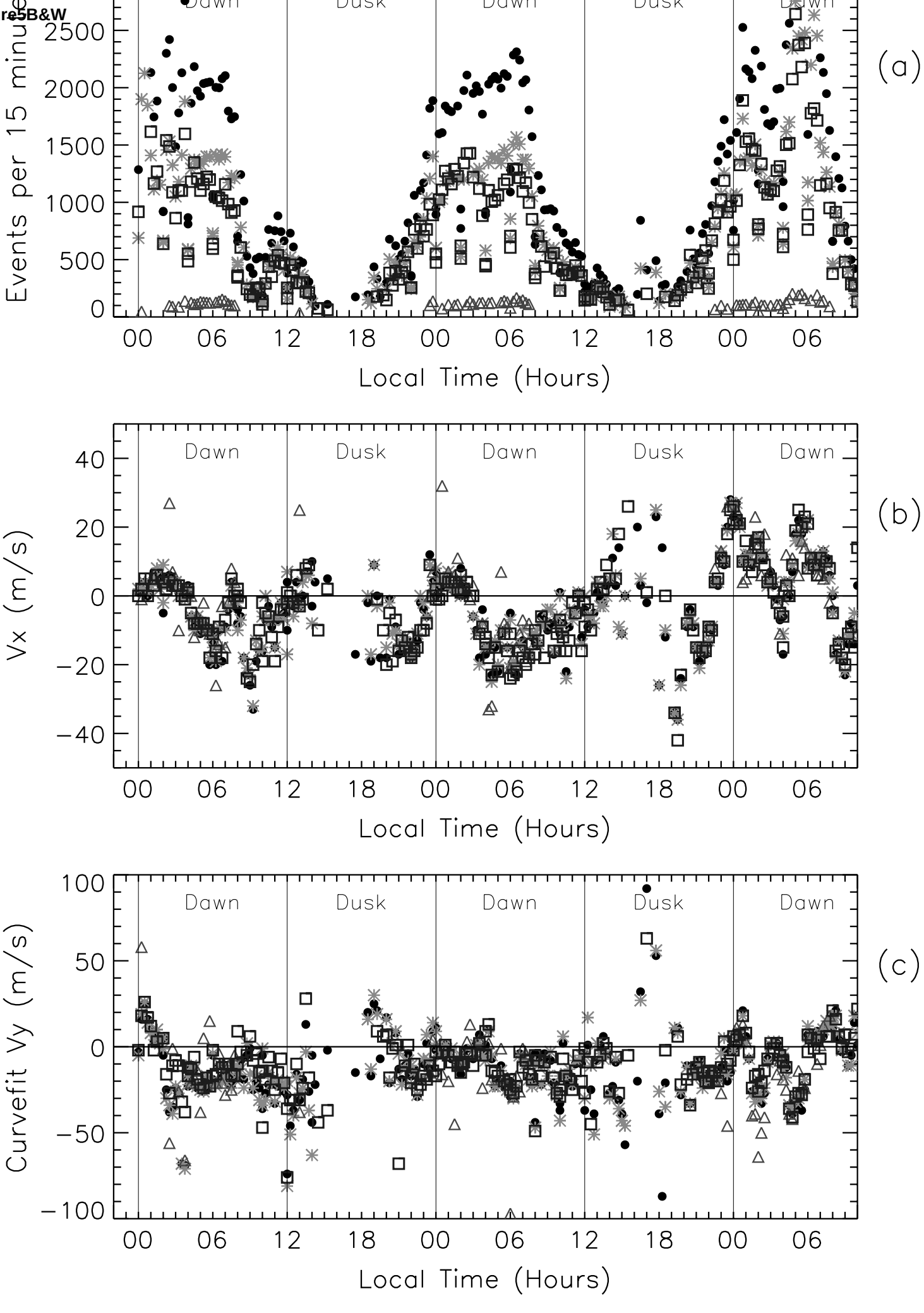
Dawn
Dusk
Dawn
Dusk
Dawn
Events per 15 minute
2500
2000
1500
1000
500
0
00
06
12
18
00
06
12
18
00
06
Local Time (Hours)
(a)
Vx (m/s)
40
20
0
−20
−40
(b)
Curvefit Vy (m/s)
100
50
0
−50
−100
(c)